Eur. Phys. J. C (2015) 75:95
DOI 10.1140/epjc/s10052-015-3319-7

THE EUROPEAN PHYSICAL JOURNAL C

Regular Article - Theoretical Physics

A heuristic description of high-p_T hadron production in heavy ion collisions

Jan Nemchik[1,2], **Roman Pasechnik**[3,a], **Irina Potashnikova**[4,5]

[1] Czech Technical University in Prague, FNSPE, Břehová 7, 11519 Prague, Czech Republic
[2] Institute of Experimental Physics SAS, Watsonova 47, 04001 Košice, Slovakia
[3] Department of Astronomy and Theoretical Physics, Lund University, 223 62 Lund, Sweden
[4] Departamento de Física, Universidad Técnica Federico Santa María, Valparaíso, Chile
[5] Centro Científico-Tecnológico de Valparaíso, Casilla 110-V, Valparaíso, Chile

Received: 10 July 2014 / Accepted: 12 February 2015 / Published online: 27 February 2015

Abstract Using a simplified model for in-medium dipole evolution accounting for color filtering effects we study the production of hadrons at large transverse momenta p_T in heavy ion collisions. In the framework of this model, several important sources of the nuclear suppression observed recently at RHIC and LHC have been analyzed. A short production length of the leading hadron l_p causes a strong onset of color transparency effects, manifesting themselves as a steep rise of the nuclear modification factor $R_{AA}(p_T)$ at large hadron p_T. The dominance of quarks with higher l_p leads to a weaker suppression at RHIC than the one observed at LHC. In the RHIC kinematic region we include an additional suppression factor, steeply falling with p_T, which is tightly related to the energy conservation constraints. This is irrelevant at LHC up to $p_T \lesssim 70$ GeV, while it causes a rather flat p_T dependence of the $R_{AA}(p_T)$ factor at RHIC c.m. energy $\sqrt{s} = 200$ GeV and even an increasing suppression with p_T at $\sqrt{s} = 62$ GeV. The calculations contain only a medium density adjustment, and for an initial time scale $t_0 = 1$ fm we found the energy-dependent maximal values of the transport coefficient, $\hat{q}_0 = 0.7, 1.0$, and $1.3\,\mathrm{GeV}^2/\mathrm{fm}$, corresponding to $\sqrt{s} = 62, 200$ GeV, and 2.76 TeV, respectively. We present a broad variety of predictions for the nuclear modification factor and the azimuthal asymmetry, which are well in agreement with available data from experiments at RHIC and LHC.

1 Introduction

The available data on high-p_T hadron production in heavy ion collisions at the LHC [1–3] and RHIC [4–7] clearly demonstrate a strong nuclear suppression exhibiting rather different features at various c.m. energies. The nuclear modification factor R_{AA} measured at the LHC reaches significantly smaller values than those at RHIC. Simultaneously, the $R_{AA}(p_T)$ factor steeply rises with p_T at the LHC, while it exhibits a rather flat p_T dependence at RHIC c.m. energy $\sqrt{s} = 200$ GeV and even a significant fall at $\sqrt{s} = 62$ GeV.

An explanation of the observed high-p_T suppression may be connected to our understanding of the hadronization phenomenon [8], namely, an energy-loss scenario of a created color parton after a heavy ion collision discussed in detail e.g. in Ref. [9] (see also Sects. 2 and 3). Production of such a parton with a high transverse momentum initiates the hadronization process, which is finalized by the formation of a jet of hadrons. In this paper, we are focused on a specific type of jets when the main fraction z_h of the jet energy E is carried by a single (leading) hadron. Here z_h of the detected hadron cannot be measured. However, the convolution of the jet momentum dependence and the hadron fragmentation leads to typically large values $z_h \gtrsim 0.5$ [9], as demonstrated in Sect. 3 (see also Fig. 5). The initial virtuality of the jet is of the same order as its energy scale. Thus at large jet energies a significant dissipation of energy via gluon radiation takes place. The latter presumably happens at an early stage of hadronization at small space-time separations (see e.g. Ref. [9]).

There are two time scales controlling the hadronization process [8,10] as is discussed in Sect. 2. The first scale is connected to the energy conservation in hadron production at large z_h. The latter scale controls production of a colorless dipole configuration at late stages of hadronization which is called sometimes a "pre-hadron" or QCD dipole. The formation of such a "pre-hadron" effectively terminates the radiative energy dissipation into gluon emissions.

[a] e-mail: Roman.Pasechnik@thep.lu.se

The corresponding length scale l_p called the production length was calculated earlier in [9,11] within a perturbative hadronization model. As will be shown in Sect. 3 (see also Fig. 6) this length scale appears to be short such that the formation of a "pre-hadron" may happen in the medium. Besides, this length appears to be weakly dependent on dipole p_T as a result of two main effects working in the opposite directions. Indeed, while the Lorentz factor effectively stretches the l_p scale at larger p_T, an increase of the energy-loss rate with p_T, oppositely, causes a shortening of l_p.

The short l_p scale means that the produced colorless dipole (hadronic state) has to survive during its propagation in the medium, otherwise it cannot be detected. Evolution of such a dipole while it propagates in the medium up to the moment of formation of the final-state hadronic wave function is controlled by the second time scale called the formation time t_f (or formation length l_f) as is discussed in Refs. [8,9] and also in Sect. 2. Here the color transparency (CT) mainly controls the surviving probability of the propagating dipole since the medium appears to be more transparent for smaller dipoles [12]. A relation between the transport coefficient which characterizes the medium density and the universal dipole cross section has been found in Refs. [13,14]. So the transport coefficient can be probed by observable effect of dipole attenuation. For our previous work on this topic, see Ref. [9].

The CT effect in production of high-p_T hadrons in heavy ion collisions was calculated within a rigorous quantum-mechanical description based on the path-integral formalism in Ref. [9]. In order to avoid complicated numerical calculations but to retain a simple physical understanding of the main features of underlying dynamics, in the present paper we start from a simplified model of Ref. [15]. Further, we generalize this model also for non-central heavy ion collisions at various energies with different contributions of quark and gluon jets to the leading high-p_T hadron production (see Sect. 4). In addition, we incorporate the color filtering effects describing an expansion of the dipole in a medium during the formation time. We found an analytical solution of the corresponding evolution equation (4.10) for the mean dipole size. Our manifestly simple formulation enables us to study the predicted nuclear modification factor R_{AA} with respect to various data as is presented in Sect. 5. The maximal value of the transport coefficient, $\hat{q}_0$, corresponding to central heavy nuclei collisions at a fixed energy is the only free parameter of the model and it is universal and independent on a particular observable.

By a comparison with the data, we found that for initial time $t_0 = 1$ fm the values of this parameter range between $\hat{q}_0 = 0.7\,\mathrm{GeV}^2/\mathrm{fm}$ at $\sqrt{s} = 62\,\mathrm{GeV}$ and $1.3\,\mathrm{GeV}^2/\mathrm{fm}$ at $\sqrt{s} = 2.76\,\mathrm{TeV}$. These values of $\hat{q}_0$ are larger than the value found in Ref. [15] due to color filtering effects in dipole size evolution, Eq. (4.10). Simultaneously, they are only slightly smaller than those in Ref. [9] within a rigorous quantum-mechanical description. However, all the values of $\hat{q}_0$ found within both the simplified model [15] and the rigorous quantum-mechanical description [9] are smaller by an order of magnitude than in Ref. [16] where the prediction was based on the pure energy-loss approach [17] due to a shorter production length is our approach. It is worth emphasizing that our approach, based on perturbative QCD (pQCD), is irrelevant to data at small $p_T \lesssim 6\,\mathrm{GeV}$, which are dominated essentially by hydrodynamics.

At large values of $x_L \equiv x_F = 2p_L/\sqrt{s}$ and/or $x_T = 2p_T/\sqrt{s}$ we incorporate an additional effect related to the initial-state interaction (ISI) energy deficit as described in Refs. [9,10,18,19] and which is presented in Sect. 5.2. The corresponding enhanced nuclear suppression is predicted to be important in the p_T dependence of R_{AA} factor at RHIC c.m. energies $\sqrt{s} = 200\,\mathrm{GeV}$ and 62 GeV. For the LHC kinematics, this effect causes a leveling of the $R_{AA}(p_T)$ behavior at the maximal measured $p_T \gtrsim 70 \div 100\,\mathrm{GeV}$. Finally, as a complementary test of our approach, in Sect. 5.3 we compared the results on the azimuthal anisotropy of produced hadrons with the corresponding RHIC/LHC data and good agreement has been found.

2 Remarks about hadronization

The subject of hadronization has been discussed in detail during the last 20 years in numerous papers (see e.g. Refs. [8–11,20–24]). Here we present the main features of nuclear suppression which differ from the popular interpretation based on the parton energy loss concept.

The production of single hadrons with high transverse momenta p_T in heavy ion collisions at high energies of RHIC [4,7] and LHC [1–3] clearly demonstrates a strong suppression compared to that in pp collisions. While there is a consensus about the source of this suppression which is due to final-state interactions with the co-moving medium created in a collision, the mechanism of such interactions is still under intensive debates.

The popular interpretation of the observed high-p_T hadron suppression is based on the loss of energy by a parton propagating through the medium created in a collision. The perturbative radiative energy loss is caused by the "wiggling" of the parton trajectory due to multiple interactions in the medium. Every time when the parton gets a kick from a scattering in the medium, a new portion of its color field is shaken off. The loss of energy induced by multiple interactions is naturally related to the broadening of the parton transverse (relative to its trajectory, i.e. to $\vec{p}_T$) momentum k_T [25,26],

$$\frac{\mathrm{d}E}{\mathrm{d}L} = -\frac{3\alpha_s}{4}\,\Delta k_T^2(L) = -\frac{3\alpha_s}{4}\int_0^L \mathrm{d}l\,\hat{q}(l), \tag{2.1}$$

where $\hat{q}(l)$ is the rate of broadening Δk_T^2, which may vary with l along the parton trajectory,

$$\hat{q}(l) = \frac{\mathrm{d}\Delta k_T^2}{\mathrm{d}l}. \tag{2.2}$$

However, the natural expectation within the energy-loss scenario that dissipation of energy by the parton in a medium should suppress production of leading hadrons raises several important questions.

In particular, one usually assumes that the energy loss induces a shift Δz_h in the argument of the fragmentation function, i.e. $z_h \Rightarrow z_h + \Delta z_h$. This could be true, if hadronization of the parton is initiated outside the medium. However, in practice it may start earlier and the main part of gluon radiation occurs at short distances right after the hard collision (see Sect. 3 and Fig. 6).

Another related assumption within the energy-loss scenario which has never been rigorously justified, is that the path of the parton propagating in the medium is assumed to be always longer than the medium size. According to this assumption the colorless hadronic state, which does not radiate energy any longer and is eventually detected, should be produced outside the medium. The validity of this assumption should further be investigated and the path length available for hadronization should be evaluated. This issue was discussed in Ref. [8] in a particular case of semi-inclusive deep-inelastic scattering (SIDIS), as well as within dynamical models of hadronization [11,22], providing rather solid constraints on the above assumption.

Besides pure theoretical arguments, the energy-loss scenario becomes problematic in explaining, for example, production of hadrons in SIDIS. The latter process provides a rigorous test for in-medium hadronization models in a more definite environment than in heavy ion collisions. Here the medium density and geometry are well known and time independent and the hadron fractional momentum z_h (the argument of the fragmentation function) has been measured. The corresponding predictions in a model including an analysis of the hadronization length [20,21], which was found rather short, were made five years prior to the measurement and then were successfully confirmed by the HERMES experiment [27,28]. The comparison with data shown in Fig. 1 (see also Ref. [8]) demonstrates rather good agreement of these predictions and the data.

On the other hand, attempts to explain the HERMES data within the energy-loss scenario were not successful. An example of comparison of the model [29] with the data [28] is depicted in Fig. 2. Such a comparison clearly demonstrates that the model fails to explain the data at large $z_h > 0.5$ which dominates the high-p_T hadron production in heavy ion collisions (see Fig. 5). Even adjustments of the transport coefficient $\hat{q}$ (actually well known for the cold nuclear matter studies [14,30]) do not improve the situation.

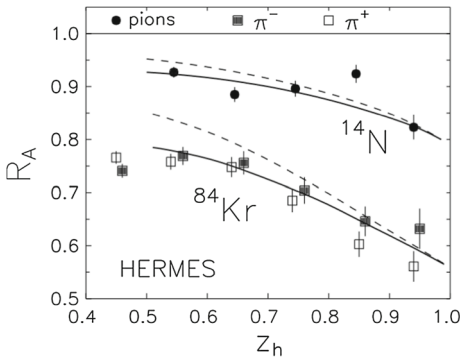

Fig. 1 A comparison of the predicted [8,20,21] z_h-dependence of the nuclear suppression factor in inclusive electroproduction of pions with the HERMES data [27,28]. *Solid* and *dashed curves* show the results with and without energy-loss corrections, respectively

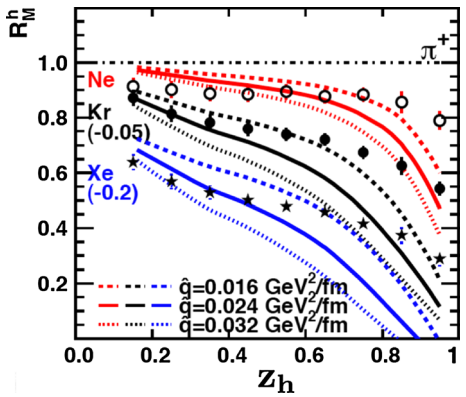

Fig. 2 The results of description of the HERMES data by the model [29] based on the energy-loss scenario, i.e. assuming a long time of hadronization. The *curves* for several values of the transport coefficient are presented

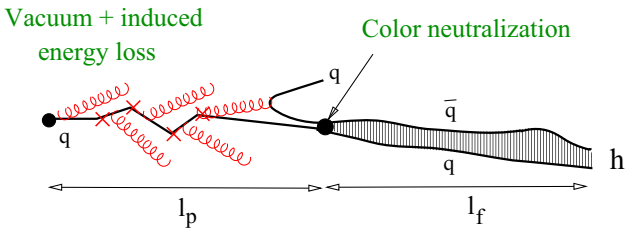

Fig. 3 Space-time development of hadronization of a highly virtual quark producing a leading hadron carrying a substantial fraction z_h of the initial light-cone momentum

Thus, the assumption of a long hadronization length should be checked more carefully and thoroughly. The basic space-time scales of the in-medium hadronization process are indicated schematically in Fig. 3. The quark regenerating its color field, which has been stripped off in a hard scattering, intensively radiates gluons and dissipates its energy, either in vacuum or in a medium. Multiple interactions in the medium induce an additional, usually less intensive, radiation. The loss of energy ceases at the moment called the production

time t_p (or production length $l_p \equiv t_p$) when the quark picks up an antiquark neutralizing its color. Thus, the production length l_p is actually the distance at which the color neutralization occurs and a colorless dipole (also called "pre-hadron") is produced and starts developing a wave function. The produced colorless dipole has yet neither hadron wave function nor hadron mass, and it takes the formation time t_f to develop both. So this process is characterized by the formation length, which usually is rather long, $l_f \sim 2E/(m_{h^*}^2 - m_h^2)$ [8,31].

The hadronization mechanism covers only the first stage of hadron production. In what follows, we concentrate on the production length scale l_p, which is the only path available for energy loss. The formation stage is described within the path-integral method in Ref. [9] and is treated within the simplified model in Sect. 4.

Notice that the question whether the hadronization occurs inside or outside the medium might have no definite answer. Indeed, there is a typical quantum-mechanical uncertainty such that the production amplitudes with different values of l_p interfere. Such an interference has been studied in Ref. [32] for SIDIS and a noticeable effect has been found. An extension of those results for a hot medium is a big challenge, so in what follows we disregard the interference and employ instead the effective standard semi-classical space-time picture of the hadronization process.

3 Radiative energy loss in vacuum

First of all, one should discriminate between vacuum and medium-induced radiative energy loss. High-p_T partons radiate gluons and dissipate energy even in vacuum, and the corresponding rate of energy loss may considerably exceed the medium-induced value Eq. (2.1) because the former is caused by a hard collision.

3.1 Regeneration of the parton color field

A high-p_T scattering of partons leads to an intensive gluon radiation in forward-backward directions, in which the initial color field of the partons is shaken off due to the strong acceleration caused by the hard collision. The radiated gluons accompanying the colliding partons do not survive the hard interaction and lose their coherence up to transverse momenta $k_T \lesssim p_T$. Therefore, the produced high-p_T parton is lacking this part of the field and starts regenerating it via radiation of a new cone of gluons which are aligned along the new direction. One can explicitly see the two cones of gluon radiation in the Born approximation calculated in Ref. [33]. This process lasts for a long time proportional to the jet energy ($E \approx p_T$).

Let such a jet be initiated by a quark. Then the coherence length (or time) l_g of the gluon radiation depends on the gluon fractional light-cone momentum β and its transverse momentum k_T relative to the jet axis as

$$l_g = \frac{2E}{M_{qg}^2 - m_q^2} = \frac{2E\beta(1-\beta)}{k_T^2 + x^2 m_q^2}, \tag{3.1}$$

where M_{qg} is the invariant mass of the recoil quark and radiated gluon system. Then using Eq. (3.1) one can trace how much energy is lost over the path length L via gluons which have lost their coherence (i.e. were radiated) during this time interval,

$$\frac{\Delta E(L)}{E} = \int_{\Lambda^2}^{Q^2} \mathrm{d}k_T^2 \int_0^1 \mathrm{d}\beta\, \beta\, \frac{\mathrm{d}n_g}{\mathrm{d}\beta\, \mathrm{d}k_T^2} \Theta(L - l_g), \tag{3.2}$$

where $Q^2 \sim p_T^2$ is the initial quark virtuality; the infra-red cutoff is fixed at $\Lambda = 0.2\,\mathrm{GeV}$ and the radiation spectrum reads

$$\frac{\mathrm{d}n_g}{\mathrm{d}x\, \mathrm{d}k_T^2} = \frac{2\alpha_s(k_T^2)}{3\pi\, \beta} \frac{k_T^2[1 + (1-\beta)^2]}{[k_T^2 + \beta^2 m_q^2]^2}. \tag{3.3}$$

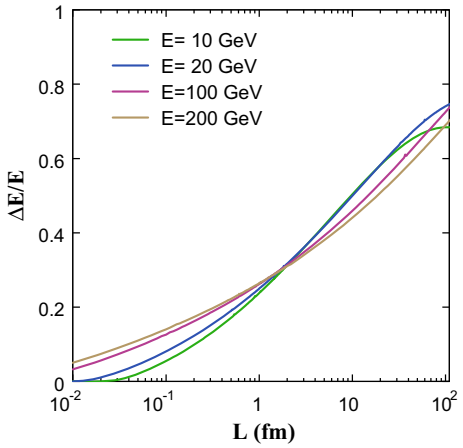

Fig. 4 The fractional energy loss by a quark with different initial energies in vacuum vs. path length L

Figure 4 shows the fractional vacuum energy loss by a quark vs. distance from the hard collision for several initial energies 10, 20, 100, and 200 GeV (compare with heavy flavors in Ref. [23]). The energy dissipation rate is considerable and energy conservation may become an issue for a long path length if one wants to produce a leading hadron. Indeed, the production rate of high-p_T hadrons is determined by a convolution of the parton distributions in the colliding hadrons (which suppresses large fractional momenta β at high p_T) with the transverse momentum distribution in the hard parton collisions (also suppresses large p_T) and with the fragmentation function $D(z_h)$ of the produced parton. The latter has a maximum at small $z_h \ll 1$, which, however, is strongly suppressed by the convolution, pushing the maximum toward large values of z_h.

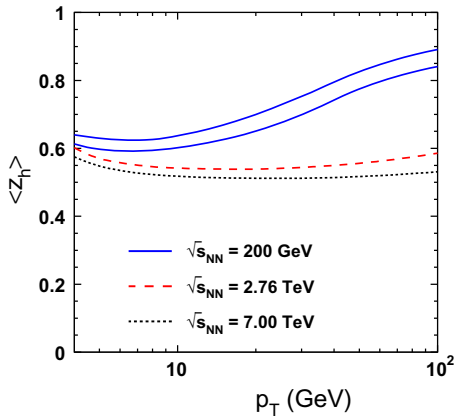

Fig. 5 The mean fraction $\langle z_h \rangle$ of the jet energy carried by a hadron detected with transverse momentum p_T. The calculations are performed for collision energies $\sqrt{s} = 0.2,\ 2.76$, and 7 TeV

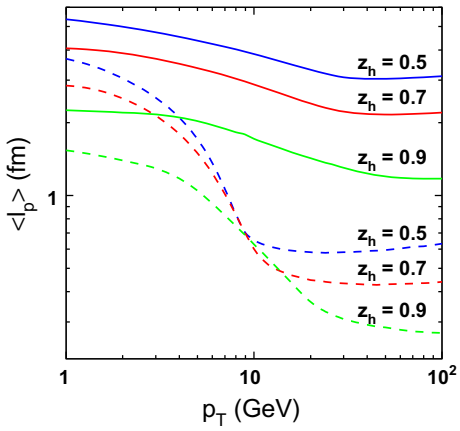

Fig. 6 The mean production length as function of energy for quark (*solid curves*) and gluon (*dashed curves*) jets. In both cases the curves are calculated at $z_h = 0.5,\ 0.7,\ 0.9$ (from *top* to *bottom*)

Numerical results of the convolution for the mean value $\langle z_h \rangle$ [9,15] are depicted in Fig. 5, separately for quark and gluon jets (upper and bottom solid curves) and at different energies, $\sqrt{s} = 200,\ 2760$, and 7000 GeV. We see that the lower is the collision energy, the larger is $\langle z_h \rangle$, especially at high p_T, since the parton k_T distribution gets steeper. For LHC energies the magnitude of $\langle z_h \rangle$ practically saturates as a function of $\sqrt{s}$ and p_T, and becomes indistinguishable for quark and gluonic jets.

We would like to emphasize the difference between inclusive production of a high-p_T hadron and a high-p_T jet. According to the discussion above, in the former case the detected hadron carries the main fractional light-cone momentum z_h of the parent jet energy. In the latter case, only the whole jet transverse momentum $p_T^{\rm jet}$ is required to be large and no other constraints are imposed. Then the fractional momenta of hadrons in the jet are typically very low, so energy conservation does not cause any severe constraints on the hadronization time scale, which increases with p_T and may be rather large.

3.2 How long does it take to produce a hadron?

Production of a hadron with a large fractional momentum z_h becomes impossible when the parton radiates a substantial fraction of its initial energy E, $\Delta E/E > 1 - z_h$. Thus, energy conservation imposes an upper bound on the production length l_p. Figures 4 and 5 clearly demonstrate that such a maximal value of l_p is rather short and nearly independent of p_T. The latter seems to be in contradiction with the Lorentz factor, which should lead to $l_p \propto p_T$. However, the intensity of gluon radiation and the energy dissipation rate rise as well, approximately as p_T^2, leading to an opposite effect to the l_p decrease.

More precisely, the p_T dependence of $\langle l_p \rangle$ can be derived within a dynamic model of hadronization. It was done in Ref. [11,15] employing a perturbative treatment of hadronization [22]. Some numerical results are plotted in Fig. 6 for fragmentation of quarks and gluons by solid and dashed curves, respectively. We see that the mean production length is rather short and slowly decreases with p_T. The production length for gluon jets is shorter due to a more intensive vacuum energy loss and a stronger Sudakov suppression, which leads to a reduction of $\langle l_p \rangle$.

The production length in Fig. 6 demonstrates a decreasing trend with p_T, which is in variance with the naive expectation of a rise due to the Lorentz factor. As explained above, this happens due to the growing virtuality and radiative dissipation of energy.

Note, so far we have taken into consideration only the energy dissipation in vacuum. Apparently, by adding the medium-induced energy loss one can only enhance the energy deficit and make the production length even shorter.

4 In-medium dipole evolution: a detailed description

The dipole attenuation and evolution is a dense medium has for the first time been studied in the framework of a sophisticated path-integral approach in Ref. [9]. Here we follow the same notations and develop a much simplified heuristic description of the dipole dynamics in the medium additionally incorporating the color filtering effects in high-p_T hadron production. The suggested approach accounts for all the major physical effects in a transparent manner while being very simple to use in practice and having a single adjustable parameter—the maximal value of the transport coefficient characterizing the medium properties.

In vacuum (e.g. in pp collisions), in evaluations of the invariant cross section of inclusive hadron production we use the model of Ref. [34]:

$$\frac{\mathrm{d}\sigma_{pp}}{\mathrm{d}y\,\mathrm{d}^2p_T} = K\sum_{i,j,k,l}\int \mathrm{d}x_i\mathrm{d}x_j\mathrm{d}^2k_{iT}\mathrm{d}^2k_{jT}F_{i/p}(x_i,k_{iT},Q^2) \times F_{j/p}(x_j,k_{jT},Q^2)\frac{\mathrm{d}\sigma}{\mathrm{d}\hat{t}}(ij\to kl)\frac{1}{\pi\, z_h}D_{h/k}(z_h,Q^2), \tag{4.1}$$

which corresponds to the collinear factorization expression modified by an intrinsic transverse momentum dependence. In Eq. (4.1), $\mathrm{d}\sigma(ij\to kl)/\mathrm{d}\hat{t}$ is the hard scattering cross section, and we follow the notations in Ref. [34]. Then the distribution in k_T reads

$$F_{i/p}(x,k_T,Q^2) = F_{i/p}(x,Q^2)\; g_p(k_T,Q^2), \tag{4.2}$$

where

$$g_p(k_T,Q^2) = \frac{1}{\pi\left\langle k_T^2(Q^2)\right\rangle}\, e^{-k_T^2/\left\langle k_T^2(Q^2)\right\rangle}. \tag{4.3}$$

The dependence of $\left\langle k_T^2(Q^2)\right\rangle$ on Q^2 scale was suggested in Ref. [34] as follows: $\langle k_T^2\rangle_N(Q^2) = 1.2\,\mathrm{GeV}^2 + 0.2\alpha_s(Q^2)Q^2$. We use the phenomenological parton distribution functions (PDFs) $F_{i/p}(x,Q^2)$ from the MSTW08 leading order (LO) fits [35]. For the fragmentation function $D_{h/k}(z_h,Q^2)$ we rely on the LO parametrization given in Ref. [36,37]. As was explicitly checked in Ref. [9], this model describes well the data on p_T-dependence of pion production in pp collisions at $\sqrt{s} = 200\,\mathrm{GeV}$ and charged hadron production at $\sqrt{s} = 7\,\mathrm{TeV}$.

The produced leading hadron carries a significant fraction $z_h \gtrsim 0.5$ of the initial light-cone parton momentum [9] as discussed in the previous Sect. 3 and presented in Fig. 5. The energy conservation requires that the hadronization process should be terminated promptly by the color neutralization, i.e. by production of a colorless "pre-hadron" (dipole), otherwise the leading parton loses too much of its energy, so that it becomes unable to produce a hadron with a large z_h fraction any longer. The corresponding time scale for production of a colorless dipole is thereby rather short and practically does not rise with p_T, as demonstrated in Fig. 6.

In comparison with the vacuum case, the multiple interactions of the parton in a dense medium induce an extra energy loss. The latter reduces the production time even more [8]. Thus, this effect enables us to calculate the corresponding survival probability function W this is the probability for a "pre-hadron" to leave the dense medium. This is according to the CT effect [12] when the attenuation rate of a dipole depends on the dipole separation r quadratically at $r\to 0$, i.e.

$$\frac{\mathrm{d}W}{\mathrm{d}l}|_{r\to 0} = -\frac{1}{2}\,\hat{q}(l)\,r^2, \tag{4.4}$$

where the rate of broadening $\hat{q}(l)$ given by Eq. (2.2) is typically called the transport coefficient, which determines the properties of the medium (see e.g. Refs. [25,26]). Here we rely on the widely used naive model for $\hat{q}$ which is taken to be dependent on the number of participants $n_{part}(\vec{b},\vec{\tau})$, on impact distance b, and on the length scale l as follows [38]:

$$\hat{q}(l,\vec{b},\vec{\tau}) = \frac{\hat{q}_0\, l_0}{l}\,\frac{n_{\mathrm{part}}(\vec{b},\vec{\tau})}{n_{\mathrm{part}}(0,0)}\,\Theta(l-l_0), \tag{4.5}$$

where $\vec{b}$ and $\vec{\tau}$ are the impact parameters of nuclear collision and the hard scattering, respectively. The variable $\hat{q}_0$ here represents the broadening rate corresponding to quark production at impact distance $\tau = 0$ in a central collision with $b = 0$ at the moment of time $t_0 = l_0$. The transport coefficient for a gluon is by a factor of 9/4 larger due to the Casimir factor C_A/C_F, where for $N_c = 3$ the factors $C_A = N_c = 3$ and $C_F = (N_c^2-1)/2\,N_c = 4/3$ are the strength of the gluon self-coupling and a gluon's coupling to a quark, respectively. The results are practically not sensitive to model-dependent t_0, and we fix it naively at $t_0 = 1.0\,\mathrm{fm}$, which is sufficient for our purposes here. Then, high-p_T hadron production is considered as a probe for the medium properties via the single fitted parameter $\hat{q}_0$ in Eq. (4.5), which depends on energy and atomic number A of the colliding nuclei.

The dipole in initial state has a small separation $r\sim 1/k_T$. During its propagation through the medium, it expands with a rate determined by the corresponding uncertainty principle $dr/dt = k_T(t)[1/\alpha p_T + 1/(1-\alpha)p_T] \propto 1/r(t)$ (for more details see Refs. [9,15,39,40]). Then the function $r(l)$ is given by

$$\frac{\mathrm{d}r}{\mathrm{d}l} = \frac{1}{r(l)E_h\alpha(1-\alpha)}. \tag{4.6}$$

Here the quark momentum fraction in the dipole is α, and $E_h = p_T$ is the dipole (hadron) energy. The solution of Eq. (4.6) is given by

$$r^2(l) = \frac{2l}{\alpha(1-\alpha)p_T} + r_0^2, \tag{4.7}$$

which is then used in (4.4) for analysis of medium attenuation of the dipole determined by $\hat{q}$,

$$R_{AB}(\vec{b},\vec{\tau},p_T) = \int_0^{2\pi}\frac{\mathrm{d}\phi}{2\pi}\exp\left[-\frac{4}{p_T}\int_L^\infty \mathrm{d}l\, l\,\hat{q}(l,\vec{b},\vec{\tau}+\vec{l})\right]. \tag{4.8}$$

This expression represents the attenuation factor for a dipole propagating in a dense medium. This dipole has been produced by a high-k_T parton (with $k_T = p_T/z_h$) at impact distance $\vec{\tau}$ in a heavy nuclei A and B collision happening at impact distance $\vec{b}$. The lower integration limit is given by $L = \max\{l_p, l_0\}$, while the transport coefficient is found from Eq. (4.5). Finally, in this calculation we employ the

Berger approximation [42] and take a symmetric dipole configuration with $\alpha \simeq 1/2$ where the projected hadron wave function is at maximal value [41].

Integrating Eq. (4.8) over the impact parameter $\vec{\tau}$ of the hard collision one obtains the nuclear modification factor for inclusive high-p_T hadron production in heavy ion $A+B$ collision at relative impact parameter b,

$$R_{AB}(\vec{b},\, p_T) = \frac{\int \mathrm{d}^2\tau\; T_A(\tau) T_B(\vec{b}-\vec{\tau}) R_{AB}(\vec{b},\vec{\tau},\, p_T)}{\int \mathrm{d}^2\tau\; T_A(\tau) T_B(\vec{b}-\vec{\tau})}. \tag{4.9}$$

This simplified approach was first employed in Ref. [15] and provides a rather good description of the first data from the ALICE experiment [43] for central collisions assuming the gluon jets contribution to leading hadron production only. Eqs. (4.8) and (4.9) generalize this simplified model making it suitable also for the analysis of suppression at different centralities. Such an analysis at smaller RHIC energies requires an additional contribution of quark jets to leading hadron production. Consequently, the mean production length $\langle l_p \rangle$ is different for quark and gluon jets as demonstrated in Ref. [9]. Therefore, the numerator in Eq. (4.9) is calculated separately for quark and gluon jets whose contributions are then summed up with the weights given by Eq. (4.1).

Although this simplified heuristic model allows one to understand the main features of the underlying dynamics, Eq. (4.6) does not describe the expansion of the dipole in a medium where the color filtering effects modify the path/length dependence of the mean dipole separation. Namely, dipoles of large size are strongly absorbed, while small dipoles attenuate less. Correspondingly, the mean transverse separation in a dipole propagating in a medium should be smaller than in vacuum. Introducing an absorptive term we arrive at a modified evolution equation,

$$\frac{\mathrm{d}r^2}{\mathrm{d}l} = \frac{2}{E_h \alpha(1-\alpha)} - \frac{1}{2} r^4(l)\, \hat{q}(l), \tag{4.10}$$

which is solved analytically with respect to an explicit form for the mean dipole size squared,

$$r^2(l) = 2\,X\,l\,\Theta(l_0-l) - \Theta(l-l_0)\,\frac{\sqrt{Zl}}{Y} \times \frac{I_1(\sqrt{Zl})\left(Z\,l_0\,K_0(\sqrt{Zl_0})/2 + \sqrt{Z\,l_0}\,K_1(\sqrt{Zl_0})\right) + \left(Z\,l_0\,I_0(\sqrt{Zl_0})/2 - \sqrt{Z\,l_0}\,I_1(\sqrt{Zl_0})\right)K_1(\sqrt{Zl})}{I_0(\sqrt{Zl})\left(Z\,l_0\,K_0(\sqrt{Zl_0})/2 + \sqrt{Z\,l_0}\,K_1(\sqrt{Zl_0})\right) + \left(Z\,l_0\,I_0(\sqrt{Zl_0})/2 - \sqrt{Z\,l_0}\,I_1(\sqrt{Zl_0})\right)K_0(\sqrt{Zl})}, \tag{4.11}$$

where we neglect the initial dipole size r_0, $\Theta(x)$ represents the step function; $I_0(x)$, $I_1(x)$, $K_0(x)$, and $K_1(x)$ are the modified Bessel functions and factors $X = 1/\alpha(1-\alpha)p_T$, $Y = \hat{q}(l)l$ with $Z = 4XY$.

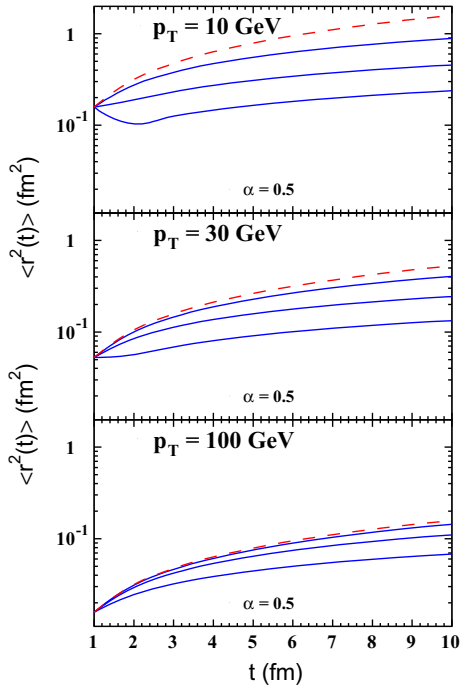

Fig. 7 Time evolution of the mean dipole size squared at $p_T = 10$, 30 and 100 GeV. *Dashed* and *solid curves* are computed within the simplified model without [Eq. (4.7)] and with [Eq. (4.10)] color filtering effects, respectively. *Solid curves* are computed for different fixed values of $\hat{q}_0 = 0.1$, 0.5 and 2.0 GeV^2/fm from *top* to *bottom*

In comparison with Eq. (4.6), the color filtering effects in Eq. (4.10) result in a reduction of the mean dipole size demonstrated in Fig. 7 for fixed values of $p_T = 10$, 30 and 100 GeV. Here we fix $\alpha = 1/2$ again [42]. Such a reduction makes the medium more transparent and depends strongly on $\hat{q}_0$. The larger is $\hat{q}_0$, the stronger is the reduction. Figure 7 also demonstrates that the reduction gradually decreases with an increase of p_T. Correspondingly, we should expect that the analysis of ALICE data performed in Ref. [15] should lead to an underestimated medium density, i.e. to a smaller parameter $\hat{q}_0$.

As was mentioned in Sect. 2, in the short length between l_0 and $l = l_p > l_0$ in the medium the parton undergoes multiple interactions. These trigger additional gluon radiation and consequently an extra energy loss [25,26]. The corresponding expression for energy loss comes from Eq. (2.1) and reads

$$\Delta E = \frac{3\alpha_s}{4}\,\Theta(l_p - l_0)\int_{l_0}^{l_p} \mathrm{d}l \int_{l_0}^{l} \mathrm{d}l'\,\hat{q}(l'). \tag{4.12}$$

Although this is a small correction, we have explicitly included it in the calculations by making a proper shift of the variable z_h in the fragmentation function.

5 Numerical results vs. data

Here we compare results of our simple model including the color filtering effects with numerous data available from the recent precision measurements at RHIC and LHC.

5.1 Hadron quenching at high-p_T

A comparison of the $R_{AA}(b=0,\,p_T)$ factor calculated above in the framework of considered model with the first data from the ALICE experiment [43] at $\sqrt{s} = 2.76\,\mathrm{TeV}$ was performed in Ref. [15]. The maximal value of the transport coefficient was adjusted to these data and fixed at $\hat{q}_0 = 0.4\,\mathrm{GeV}^2/\mathrm{fm}$. The growing p_T-dependence of $R_{AA}(p_T)$ follows from the reduction of the mean dipole size at higher p_T [in accordance with Eq. (4.7)] and due to a Lorentz dilation of the dipole size expansion. This leads to a more transparent medium for more energetic smaller dipoles in accordance with the CT effect. An analogous growing energy dependence of the medium transparency was predicted and observed in the case of virtual photoproduction of vector mesons on nuclei [44,45].

Being encouraged by the first success of the simplified model, we have generalized this model for studies of production of various high-p_T hadrons at distinct energies by incorporating additional quark jet contributions to leading hadron production besides gluon ones with relative weights given by Eq. (4.1). The original treatment, which was suitable only for central heavy ion collisions, has now been extended also to non-central collisions. Moreover, for the first time we have incorporated also the color filtering effects in the evolution equation for the mean dipole size, Eq. (4.10).

The results for central (0–5 %) Pb–Pb collisions at $\sqrt{s} = 2.76\,\mathrm{TeV}$ are shown by a dashed curve in Fig. 8, compared to the ALICE data [1] and CMS [2,3]. The only free parameter, the maximal value of the transport coefficient defined in Eq. (4.5), was adjusted to the data and fixed at $\hat{q}_0 = 1.3\,\mathrm{GeV}^2/\mathrm{fm}$ corresponding to the mean value of the impact parameter $\langle b\rangle = 2.3\,\mathrm{fm}$. This value of the transport coefficient is then valid for all further calculations for Pb–Pb collisions at c.m. energy $\sqrt{s} = 2.76\,\mathrm{GeV}$.

Note that, while our calculations describe well the data at high $p_T \gtrsim 6\,\mathrm{GeV}$, the region of smaller p_T is apparently dominated by thermal mechanisms of hadron production.

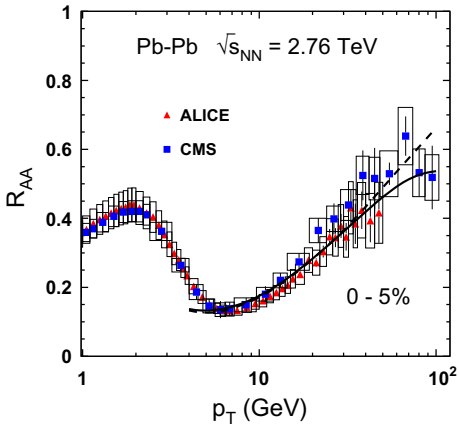

Fig. 8 The nuclear modification factor $R_{AA}(p_T)$ for charged hadron production in central (with centrality 0–5 %) Pb–Pb collisions at $\sqrt{s} = 2.76\,\mathrm{TeV}$. The dashed line represents the simple model prediction given by Eqs. (4.4), (4.11), (4.9), and the space- and time-dependent transport coefficient (4.5) with the single adjustable parameter $\hat{q}_0 = 1.3\,\mathrm{GeV}^2/\mathrm{fm}$. The *solid curve*, in addition, includes the effect of initial-state interactions in nuclear collisions [10,18] described in Sect. 5.2. The data for $R_{AA}(p_T)$ are from the ALICE [1] and CMS [2,3] measurements

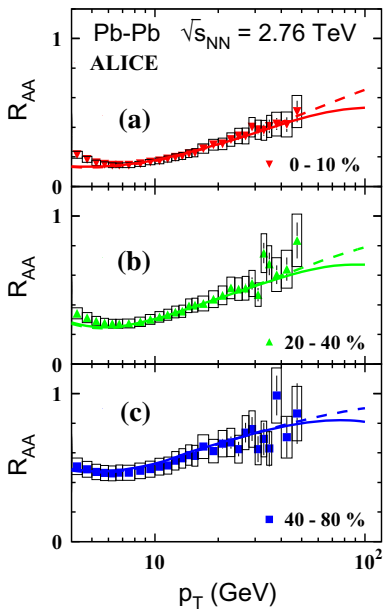

Fig. 9 The centrality dependence of the nuclear modification factor $R_{AA}(p_T, b)$ for charged hadron production measured by the ALICE experiment [1]. The intervals of centrality are indicated. The meaning of the curves is the same as in Fig. 8

The variation of the suppression factor $R_{AA}(b,\,p_T)$ with impact parameter b given by Eqs. (4.4), (4.11), and (4.9) is plotted by dashed curves and compared to the data at different centralities obtained by ALICE [1] in Fig. 9, and by CMS [2,3] in Fig. 10. In all cases we observe a rather good agreement.

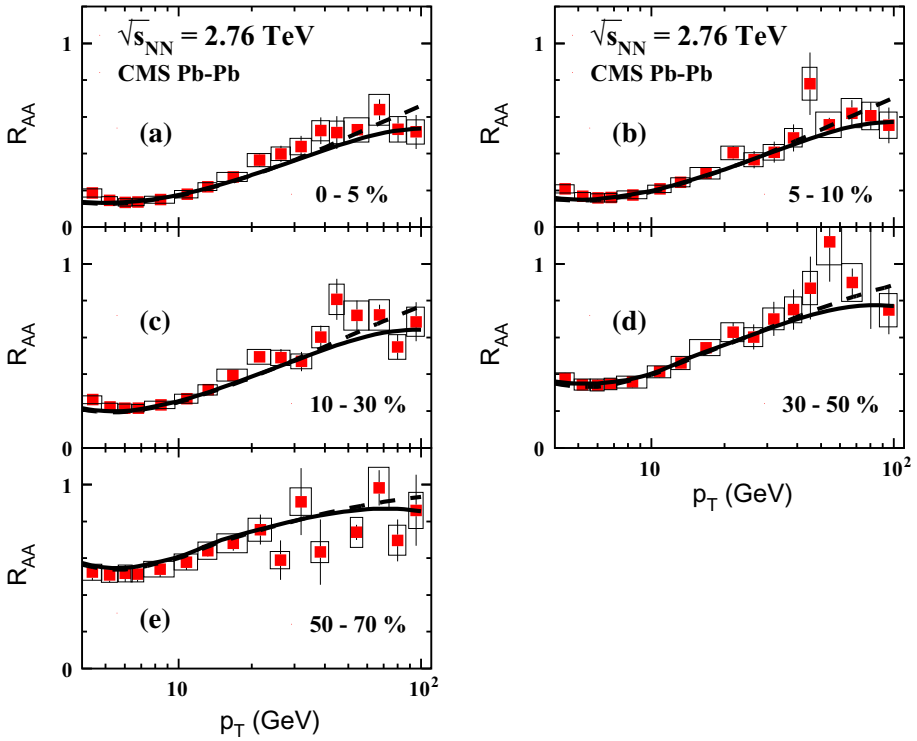

Fig. 10 The same as in Fig. 9, but with the data from CMS [2,3]

5.2 Large x_T suppression due to energy conservation

In the course of propagation through the nucleus multiple interactions of the projectile hadron and its debris lead to a dissipation of energy. The corresponding loss of energy is proportional to the energy of the projectile hadron, thus the related effects do not disappear at very high energies as was stressed in Ref. [18] (see also Ref. [46]). In the Fock state representation, the projectile hadron can be decomposed over different states, which are the fluctuations of this hadron "frozen" by Lorentz time dilation. The interaction with the target modifies the weights of Fock states since some interact stronger, some weaker.

In each Fock component the hadron momentum is shared between its constituents, and the momentum distribution depends on their multiplicity: the more constituents are involved, the smaller is the mean energy per parton. This leads to the softer fractional energy distribution of a leading parton, and the projectile parton distribution falls at $x \to 1$ steeper on a nuclear target than on a proton.

In the case of hard reaction on a nucleus, such softening of the projectile parton fractional energy distribution can be viewed as an effective energy loss of the leading parton due to initial-state multiple interactions. This leads to an enhancement of the weight factors for higher Fock states in the projectile hadron with a large number of constituents having a tough energy sharing. Consequently, the mean energy of the leading parton decreases compared to lower Fock states which dominate the hard reaction on a proton target. Such a reduction of the mean fractional energy of the leading parton is apparently independent of the initial hadron energy and can be treated as an effective loss of energy proportional to the initial hadron energy. A detailed description and interpretation of the corresponding additional suppression was presented also in Refs. [9,19,24].

Here we would like to emphasize that this effective energy loss is different from the energy loss by a single parton propagating through a medium and experiencing induced gluon radiation. In this case the mean fractional energy carried by the radiated gluons vanishes at large initial energies E as $\Delta E/E \propto 1/E$ [25,26,47,48].

The initial-state energy loss (ISI effect) is a minor effect at high energies and midrapidities. However, it may essentially suppress the cross section when reaching the kinematical bounds, $x_L = 2p_L/\sqrt{s} \to 1$ and $x_T = 2p_T/\sqrt{s} \to 1$. Correspondingly, the proper variable which controls this effect is $\xi = \sqrt{x_L^2 + x_T^2}$.

The magnitude of suppression was evaluated in Refs. [10, 18]. It was found within the Glauber approximation that each interaction in the nucleus leads to a suppression $S(\xi) \approx 1-\xi$. Summing up over the multiple initial-state interactions in a p-A collision with impact parameter b and relying on Eq. (4.1), one arrives at a nuclear ISI-modified PDF $F_{i/p}(x_i, Q^2) \Rightarrow F_{i/p}^{(A)}(x_i, Q^2, b)$, where

$$F^{(A)}_{i/p}(x_i, Q^2, b) = C\, F_{i/p}(x_i, Q^2) \times \frac{\left[e^{-\xi\sigma_{\rm eff}T_A(b)} - e^{-\sigma_{\rm eff}T_A(b)}\right]}{(1-\xi)\left[1 - e^{-\sigma_{\rm eff}T_A(b)}\right]}, \qquad (5.1)$$

where $\sigma_{\rm eff} = 20\,$mb [18,49] is the hadronic cross section which effectively determines the rate of multiple interactions, and constant C is given by the Gottfried sum rule. It was found that such an additional nuclear suppression due to the ISI effects represents an energy independent feature common for all known reactions, experimentally studied so far, with any leading particle (hadrons, Drell–Yan dileptons, charmonium, etc.). Following Ref. [10], in the analysis of high-p_T hadron production we apply exactly the same model developed in Refs. [18,19,24] for large x_L and with the same physical parameters.

Using PDFs modified by the ISI energy loss, Eq. (5.1), one achieved a good parameter-free description of available data from the BRAHMAS [50] and STAR [51] experiments at forward rapidities (large x_L) in dA collisions [10,18]. An alternative interpretation [52] at forward rapidities is based on the coherence effect (color glass condensate or CGC), which should disappear at lower energies because $x \propto 1/\sqrt{s}$ increases. Assuming that besides CGC there is no other mechanism contributing to the suppression observed by BRAHMS, one should not expect any suppression at smaller energies where no coherence effects are possible. However, according to Eq. (5.1) the suppression caused by the ISI energy-loss scales in Feynman $x_F = x_L$ and should exist at any energy. Thus, by reducing the collision energy one should provide a sensitive test for the models. The expectation of no suppression following from CGC at forward rapidities and small energies is in contradiction with data from the NA49 experiments [53] at SPS obtained at much smaller energy than BRAHMS. This observation confirms that the effect of suppression at forward rapidities is still there and can be explained entirely by the ISI energy loss.

Another test of the mechanism based on the ISI energy loss can be realized for RHIC energies at large p_T, where no coherence effects are expected, while the value of ξ is considerable and an ISI energy deficit should lead to a suppression at large x_T similar to what was observed at large x_L. The predictions for large-p_T suppression based on ISI effects [10] at the collision energy $\sqrt{s} = 200\,$GeV and at midrapidity are confirmed by the PHENIX data for central d–Au collisions [54] as is demonstrated in Fig. 11. No alternative explanation has been proposed so far.

The ISI energy loss also affects the p_T dependence of the nuclear suppression in heavy ion collisions. These effects are calculated similarly to p(d)-A collisions using the modified parton distribution functions Eq. (5.1) for nucleons in both colliding nuclei. Naively, at the LHC one would not expect any sizable ISI energy loss. Nevertheless, even at such high energies one can reach large x_T sufficient for the manifestation of ISI energy-loss effects. These corrections are predicted to be important for $p_T \gtrsim 70\,$GeV. This is demonstrated in Figs. 8, 9, and 10 by solid lines which show a flattening of the $R_{AA}(p_T)$ factor at large p_T.

At RHIC energies this additional suppression reduces $R_{AA}(p_T)$ significantly at large p_T as is demonstrated in Fig. 12 for central Au–Au collisions at $\sqrt{s} = 200\,$GeV. Including the CT effect only and repeating the same calculation as above for the LHC, we get R_{AA} steeply rising with p_T, as is depicted by the dashed curve. Since the parameter $\hat{q}_0$ is expected to vary with energy, it was re-adjusted and found to be $\hat{q}_0(RHIC) = 1.0\,{\rm GeV}^2/{\rm fm}$, which is less than in col-

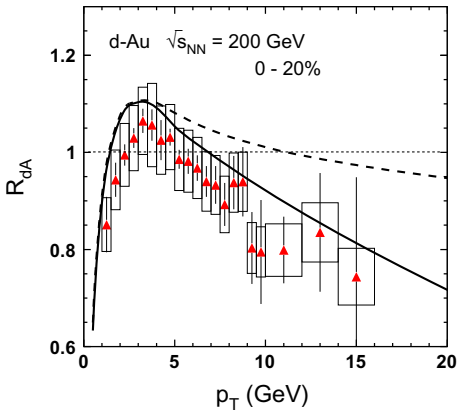

Fig. 11 The nuclear modification factor $R_{dAu}(p_T)$ for neutral pions produced in central (0–20 %) d–Au collisions at $\sqrt{s} = 200\,$GeV and $\eta = 0$. The *solid* and *dashed curves* show the predictions calculated with and without the ISI corrections, respectively. The isotopic effect is included. The data are from the PHENIX experiment [54]

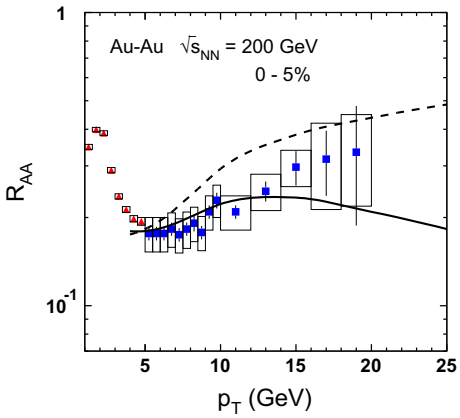

Fig. 12 The nuclear modification factor $R_{AA}(p_T)$ for neutral pions produced in central Au—Au collisions at $\sqrt{s} = 200\,$GeV. The *solid* and *dashed line* are computed with and without ISI corrections, respectively. The PHENIX data are from Refs. [4] (*triangles*) and [5] (*squares*)

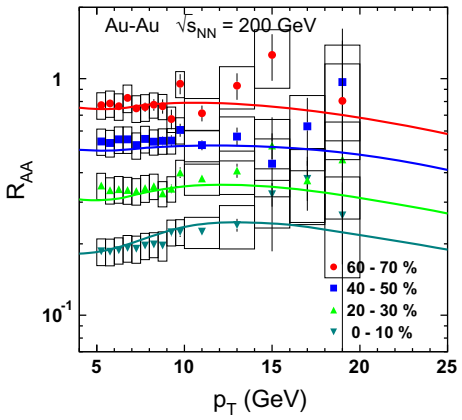

Fig. 13 The centrality dependence of the nuclear modification factor $R_{AA}(p_T, b)$ in comparison to the PHENIX data with Au–Au collisions at $\sqrt{s} = 200\,\text{GeV}$ [4]

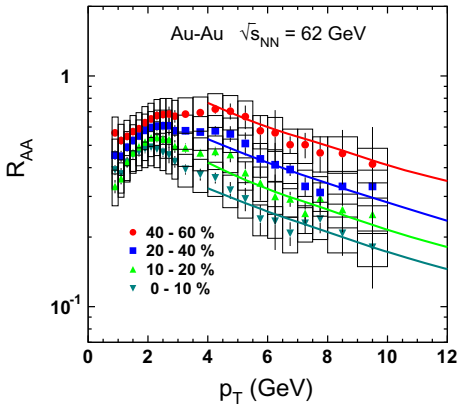

Fig. 14 The same as in Fig. 13, but at $\sqrt{s} = 62\,\text{GeV}$. The data are taken from Ref. [6]

lisions at the LHC.[1] Inclusion of the ISI effects, Eq. (5.1), leads to a sizable additional suppression, as is shown by the solid curve.

By fixing $\hat{q}_0 = 1.0\,\text{GeV}^2/\text{fm}$ we can obtain other observables for Au–Au collisions at $\sqrt{s} = 200\,\text{GeV}$. Figure 13 shows our results for the suppression of π^0 at different centralities, in comparison with the PHENIX data [4].

One achieves stronger ISI effects either by enlarging p_T at some fixed energy, or by reducing the collision energy keeping the p_T range unchanged. The latter is demonstrated by the data on $R_{AA}(p_T)$ in Au–Au collisions at smaller RHIC energy $\sqrt{s} = 62\,\text{GeV}$ in Fig. 14 showing an increasing rather than falling nuclear suppression as a direct manifestation of the ISI energy-loss effects, Eq. (5.1). Such data are important for studies of the energy-loss effects. Our calculations again demonstrate good agreement with the data. Here the hot medium properties are changed, so in order to account for that we have re-adjusted the parameter, $\hat{q}_0 = 0.7\,\text{GeV}^2/\text{fm}$.

[1] Notice that $\hat{q}_0$ is also A-dependent.

5.3 Anisotropy in azimuthal angle distribution

The observed high-p_T hadrons suppression reflects a contribution of some effective medium volume. Thus one should expect that the resulting suppression depends on the propagation length, while the direction of propagation perpendicular to the surface of the medium is preferable. This effect leads to an azimuthal asymmetry in the hadron angular distribution presumably for non-central collisions [9].

Typically, for azimuthal asymmetry one studies the second moment of the azimuthal angle distribution, i.e. $v_2 \equiv \langle\cos(2\phi)\rangle$ given by

$$v_2(p_T, b) = \frac{\int \mathrm{d}^2\tau\, T_A(\tau) T_B(\vec{b}-\vec{\tau}) \int_0^{2\pi} \mathrm{d}\phi \cos(2\phi) R_{AB}^{\phi}(\vec{b}, \vec{\tau}, p_T)}{\int \mathrm{d}^2\tau\, T_A(\tau) T_B(\vec{b}-\vec{\tau}) \int_0^{2\pi} \mathrm{d}\phi R_{AB}^{\phi}(\vec{b}, \vec{\tau}, p_T)}, \tag{5.2}$$

where $R_{AB}^{\phi}(\vec{b}, \vec{\tau}, p_T) \equiv R_{AB}(\vec{b}, \vec{\tau}, p_T, \phi)$ is given by Eq. (4.8) but without integration over ϕ. The results of this calculation are compared with ALICE [55] and CMS data [56] in Figs. 15 and 16 and are found to be in a good overall agreement.

Similarly to the data on R_{AA}, our pQCD calculations for $v_2(p_T)$ grossly underestimate the data at small $p_T \lesssim 6\,\text{GeV}$ due to the presence of two different mechanisms discussed earlier in Ref. [9]: the dominant hydrodynamic mechanism of elliptic flow, leading to a large and increasing anisotropy $v_2(p_T)$ at high p_T, which abruptly switches to the pQCD regime having a much smaller azimuthal anisotropy.

Finally, we have also evaluated the azimuthal anisotropy at smaller c.m. energies and compared with the corresponding RHIC data. Our results agree well with PHENIX data for π^0 production, which is demonstrated in Fig. 17.

6 Summary

In this paper, we contribute to a quantitative understanding of the strong nuclear suppression of leading high-p_T hadrons produced inclusively in heavy ion collisions. The main motivation comes from the improved quality of data at RHIC and new high-statistics data at LHC, which provide a strong potential for a more decisive verification of different models.

The popular pure energy-loss scenario, based on the unjustified assumption of long production length, experiences difficulties explaining the data and also fails to describe simultaneously the data from the HERMES experiment for leading hadron production in semi-inclusive DIS, which represents a sensitive testing keystone for in-medium hadronization models.

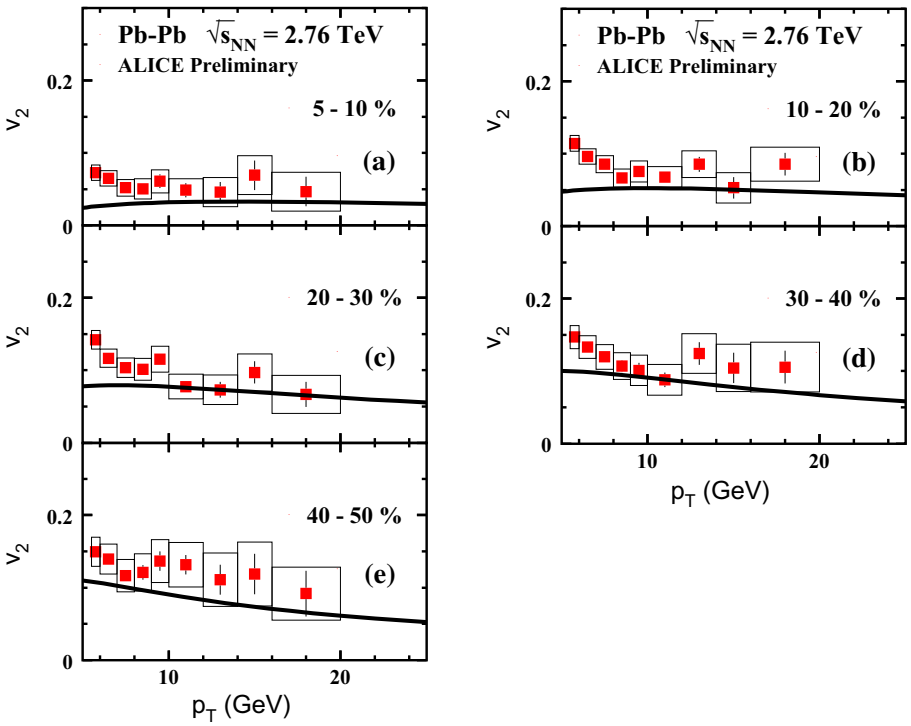

Fig. 15 The azimuthal anisotropy, v_2, vs p_T in comparison to ALICE data [55] for charge hadron production in Pb–Pb collisions at midrapidity, at $\sqrt{s} = 2.76$ TeV and at different centralities

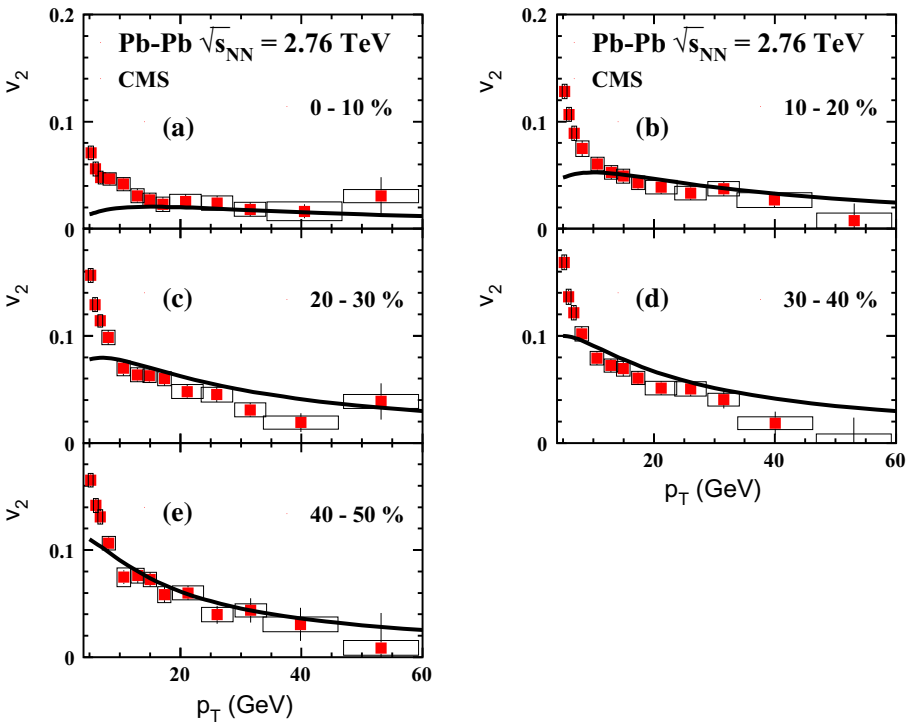

Fig. 16 The same as in Fig. 15, but with the CMS data [56]

In this work, we present an alternative mechanism for nuclear suppression in high-p_T hadron production. The key point is that the production length of leading hadrons does not rise with p_T and remains rather short as is demonstrated in Fig. 6 (see also Refs. [9,15]). This is a consequence of a strong increase of the energy dissipation by a highly virtual parton, produced in a high-p_T process, with jet energy. The production moment of a colorless hadronic state ("prehadron") ceases the energy loss. The main reason for such a suppression is related to the survival probability of the "prehadron" propagating through the dense matter. According to Eqs. (4.7) and (4.11), larger p_T's prefer a smaller dipole size and the medium becomes more transparent in accordance with the color transparency effect. The corresponding

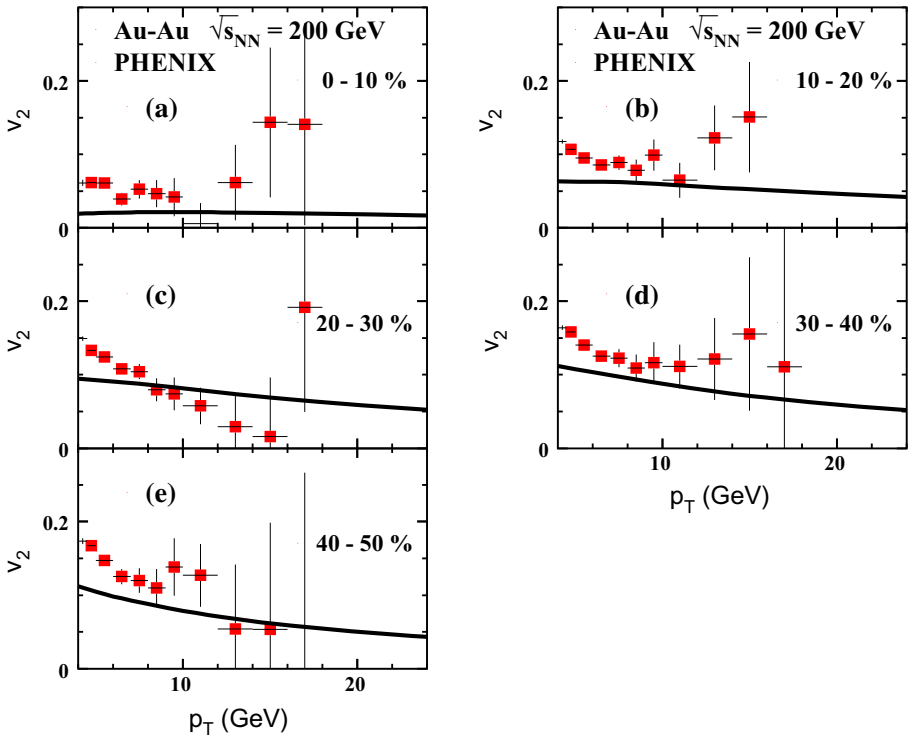

Fig. 17 The same as in Fig. 15, but with the PHENIX data [57]

increase of the nuclear suppression factor $R_{AA}(p_T)$ is indeed observed at the LHC.

Thus we conclude that the main reason for the observed suppression of high-p_T hadron production in heavy ion collisions is not an energy loss, but attenuation of early produced colorless dipoles ("pre-hadrons") propagating through a dense absorptive matter.

One should clearly discriminate between vacuum- and medium-induced energy loss. The former is much more intensive and is the main cause of shortness of the production length l_p.

One should also discriminate between the terms "jet quenching" and "hadron quenching". The latter is considered in the present paper, namely, a high-p_T hadron detected inclusively and carrying the main fraction z_h of the accompanying jet energy as is depicted in Fig. 5. This leads to smallness of the l_p scale as a consequence of constraints coming from an intensive energy loss in vacuum at large p_T and energy conservation. On the other side, if none of hadrons in the jet are forced to have a large z_h and the whole jet has a large p_T, then the hadronization lasts a long time due to the usual Lorentz time dilation.

Although the attenuation of colorless dipoles propagating through a medium has already been studied in Ref. [9] within the rigorous quantum-mechanical approach based on the Green functions formalism, in this paper we present an alternative simplified description of the high-p_T hadron production in heavy ion collisions. For this purpose, we start from the simple model of Ref. [15] and generalize it for non-central heavy ion collisions additionally including quark jet contributions to leading hadron production. In the framework of this generalized model, we have incorporated for the first time the color filtering effects in the evolution equation for the mean dipole size and found its simple analytical solution, Eq. (4.11). As the main result of this study, we found that the color filtering effects lead to a reduction of the mean dipole size as demonstrated in Fig. 7 and, consequently, to a more transparent nuclear medium.

First, we have studied the suppression factor $R_{AA}(p_T)$ in comparison to available data at various centralities and c.m. energies in corresponding RHIC and LHC kinematic domains. At large $x_T \gtrsim 0.1$ we included an additional suppression factor from the initial-state interactions. This factor, which falls steeply with p_T, causes a rather flat p_T dependence of $R_{AA}(p_T)$ function at RHIC energy $\sqrt{s} = 200\,\text{GeV}$ and even leads to an increase of suppression at high p_T at lower $\sqrt{s} = 62\,\text{GeV}$. At the next step, we evaluated the azimuthal anisotropies in hadron production at different energies and centralities corresponding to measurements at RHIC and LHC.

In all the cases we found a fair agreement with data at high p_T. The only adjustable parameter which is the maximal magnitude of the transport coefficient, was estimated between $\hat{q}_0 = 1.3\,\text{GeV}^2/\text{fm}$, $1.0\,\text{GeV}^2/\text{fm}$, and $0.7\,\text{GeV}^2/\text{fm}$ values at energies $\sqrt{s} = 2.76\,\text{TeV}$, $200\,\text{GeV}$ and $62\,\text{GeV}$, respectively, for an initial time scale $t_0 = 1\,\text{fm}$ and for such nuclei as Pb and Au. These values of $\hat{q}_0$ are larger than was found in the analysis of the first ALICE data

[15] due to the color filtering effects included in Eq. (4.10). Simultaneously, they are close to the expected magnitude $\hat{q}_0 \sim 1\,\mathrm{GeV}^2/\mathrm{fm}$ [25,26] as well as to values extracted from RHIC and LHC data by the JET Collaboration [58]. Moreover, values of $\hat{q}_0$ extracted within the simplified model are similar and only slightly smaller than those found in Ref. [9] within a rigorous quantum-mechanical description. It is worth noticing that the pure energy-loss scenario leads to the value of the transport coefficient [16], which is an order of magnitude larger than expected [25,26].

Remarkably, such a simple formulation absorbs all the important physical effects which are naturally inherited from the much more involved Green functions formalism and enables immediate comparison of its predictions to various existing data on high-p_T hadrons production in heavy ions collisions. Thus, technically our model is much more convenient for the practical use for testing of the underlined nuclear effects than far more complicated path-integral techniques.

Acknowledgments We are indebted to Boris Kopeliovich for inspiring discussions and useful correspondence. This work was supported in part by Fondecyt (Chile) Grants 1130543, 1130549 and by Conicyt-DFG Grant No. RE 3513/1-1. The work of J. N. was partially supported by the Grant 13-20841S of the Czech Science Foundation (GAČR), by the Grant MSMT LG13031, by the Slovak Research and Development Agency APVV-0050-11 and by the Slovak Funding Agency, Grant 2/0020/14.

References

1. B. Abelev et al., ALICE Collaboration, Phys. Lett. B **720**, 52 (2013)
2. Y.-J. Lee, for the CMS Collaboration, J. Phys. G **38**, 124015 (2011)
3. A.S. Yoon, for the CMS Collaboration, J. Phys. G **38**, 124116 (2011)
4. A. Adare et al., PHENIX Collaboration, Phys. Rev. C **87**, 034911 (2013)
5. M.L. Purschke, for the PHENIX Collaboration, J. Phys. G **38**, 124016 (2011)
6. PHENIX Collaboration, preliminary data posted at http://www.phenix.bnl.gov/WWW/plots/show_plot.php?editkey=p1118
7. J. Adams et al., STAR Collaboration, Phys. Rev. Lett. **91**, 072304 (2003)
8. B.Z. Kopeliovich, J. Nemchik, E. Predazzi, A. Hayashigaki, Nucl. Phys. A **740**, 211 (2004)
9. B.Z. Kopeliovich, J. Nemchik, I.K. Potashnikova, I. Schmidt, Phys. Rev. C **86**, 054904 (2012)
10. B.Z. Kopeliovich, J. Nemchik, J. Phys. G **38**, 043101 (2011)
11. B.Z. Kopeliovich, H.-J. Pirner, I.K. Potashnikova, I. Schmidt, Phys. Lett. B **662**, 117 (2008)
12. B.Z. Kopeliovich, L.I. Lapidus, A.B. Zamolodchikov, JETP Lett. **33**, 595 (1981); Pisma Zh. Eksp. Teor. Fiz. **33**, 612 (1981)
13. M.B. Johnson, B.Z. Kopeliovich, A.V. Tarasov, Phys. Rev. C **63**, 035203 (2001)
14. B.Z. Kopeliovich, I.K. Potashnikova, I. Schmidt, Phys. Rev. C **81**, 035204 (2010)
15. B.Z. Kopeliovich, I.K. Potashnikova, I. Schmidt, Phys. Rev. C **83**, 021901 (2011)
16. A. Adare et al., PHENIX Collaboration, Phys. Rev. C **77**, 064907 (2008)
17. S. Wicks, W. Horowitz, M. Djordjevic, M. Gyulassy, Nucl. Phys. A **784**, 426 (2007)
18. B.Z. Kopeliovich, J. Nemchik, I.K. Potashnikova, M.B. Johnson, I. Schmidt, Phys. Rev. C **72**, 054606 (2005)
19. J. Nemchik, V. Petracek, I.K. Potashnikova, M. Sumbera, Phys. Rev. C **78**, 025213 (2008)
20. B. Z. Kopeliovich, J. Nemchik, E. Predazzi, *Proceedings of the Workshop on Future Physics at HERA*, eds. by G. Ingelman, A. De Roeck, R. Klanner, DESY 1995/1996 (1996), vol. 2, p. 1038. nucl-th/9607036
21. B. Z. Kopeliovich, J. Nemchik, E. Predazzi, *Proceedings of the ELFE Summer School on Confinement Physics*, eds. by S. D. Bass, P. A. M. Guichon (Editions Frontieres, Cambridge, 1995), p. 391. hep-ph/9511214
22. B.Z. Kopeliovich, H.-J. Pirner, I.K. Potashnikova, I. Schmidt, A.V. Tarasov, Phys. Rev. D **77**, 054004 (2008)
23. B.Z. Kopeliovich, I.K. Potashnikova, I. Schmidt, Phys. Rev. C **82**, 037901 (2010)
24. B.Z. Kopeliovich, J. Nemchik, I.K. Potashnikova, I. Schmidt, Int. J. Mod. Phys. E **23**, 1430006 (2014)
25. R. Baier, Y.L. Dokshitzer, S. Peigne, D. Schiff, Phys. Lett. B **345**, 277 (1995)
26. R. Baier, Y.L. Dokshitzer, S. Peigne, D. Schiff, Nucl. Phys. B **484**, 265 (1997)
27. A. Airapetian et al., HERMES Collaboration, Eur. Phys. J. C **20**, 479 (2001)
28. A. Airapetian et al., HERMES Collaboration, Phys. Lett. B **577**, 37 (2003)
29. W.T. Deng, X.N. Wang, Phys. Rev. C **81**, 024902 (2010)
30. S. Domdey, D. Grunewald, B.Z. Kopeliovich, H.J. Pirner, Nucl. Phys. A **825**, 200 (2009)
31. B.Z. Kopeliovich, B.G. Zakharov, Phys. Rev. D **44**, 3466 (1991)
32. B.Z. Kopeliovich, H.-J. Pirner, I.K. Potashnikova, I. Schmidt, A.V. Tarasov, O.O. Voskresenskaya, Phys. Rev. C **78**, 055204 (2008)
33. J.F. Gunion, G. Bertsch, Phys. Rev. D **25**, 746 (1982)
34. X.-N. Wang, Phys. Rev. C **61**, 064910 (2000)
35. A.D. Martin, W.J. Stirling, R.S. Thorne, G. Watt, Eur. Phys. J. C **63**, 189 (2009)
36. D. de Florian, R. Sassot, M. Stratmann, Phys. Rev. D **75**, 114010 (2007)
37. D. de Florian, R. Sassot, M. Stratmann, Phys. Rev. D **76**, 074033 (2007)
38. X.F. Chen, C. Greiner, E. Wang, X.N. Wang, Z. Xu, Phys. Rev. C **81**, 064908 (2010)
39. B.Z. Kopeliovich, I.K. Potashnikova, I. Schmidt, Phys. Rev. C **82**, 024901 (2010)
40. B.Z. Kopeliovich, Nucl. Phys. A **854**, 187 (2011)
41. A.V. Efremov, A.V. Radyushkin, Phys. Lett. B **94**, 245 (1980)
42. E.L. Berger, Phys. Lett. B **89**, 241 (1980)
43. K. Aamodt et al., ALICE Collaboration, Phys. Lett. B **696**, 30 (2011)
44. B.Z. Kopeliovich, J. Nemchik, N.N. Nikolaev, B.G. Zakharov, Phys. Lett. B **309**, 179 (1993)
45. B.Z. Kopeliovich, J. Nemchik, N.N. Nikolaev, B.G. Zakharov, Phys. Lett. B **324**, 469 (1994)
46. F. Arleo, S. Peigne, T. Sami, Phys. Rev. D **83**, 114036 (2011)
47. F. Niedermayer, Phys. Rev. D **34**, 3494 (1986)
48. S.J. Brodsky, P. Hoyer, Phys. Lett. B **298**, 165 (1993)
49. B.Z. Kopeliovich, I.K. Potashnikova, I. Schmidt, Phys. Rev. C **73**, 034901 (2006)

50. I. Arsene et al., BRAHMS Collaboration, Phys. Rev. Lett. **93**, 242303 (2004)
51. J. Adams et al., STAR Collaboration, Phys. Rev. Lett. **97**, 152302 (2006)
52. D. Kharzeev, Y.V. Kovchegov, K. Tuchin, Phys. Lett. B **599**, 23 (2004)
53. B. Boimska, NA49 Collaboration, Ph.D. Dissertation, CERN-THESIS-2004-035. http://cds.cern.ch/record/799647?ln=en
54. S.S. Adler et al., PHENIX Collaboration, Phys. Rev. Lett. **98**, 172302 (2007)
55. A. Dobrin, for the ALICE Collaboration, J. Phys. G **38**, 124170 (2011)
56. S. Chatrchyan et al., CMS Collaboration, Phys. Rev. Lett. **109**, 022301 (2012)
57. A. Adare et al., PHENIX Collaboration, Phys. Rev. Lett. **105**, 142301 (2010)
58. K.M. Burke et al., JET Collaboration, Phys. Rev. C **90**, 014909 (2014)